

See discussions, stats, and author profiles for this publication at: <https://www.researchgate.net/publication/281142903>

Proteomic Study of Pyrrolizidine Alkaloid-Induced Hepatic Sinusoidal Obstruction Syndrome in Rats

ARTICLE *in* CHEMICAL RESEARCH IN TOXICOLOGY · AUGUST 2015

Impact Factor: 3.53 · DOI: 10.1021/acs.chemrestox.5b00113 · Source: PubMed

READS

43

11 AUTHORS, INCLUDING:



[Yan Hong Li](#)

The Chinese University of Hong Kong

4 PUBLICATIONS 8 CITATIONS

[SEE PROFILE](#)



[William Tai](#)

The Hong Kong Polytechnic University

23 PUBLICATIONS 220 CITATIONS

[SEE PROFILE](#)



[Junyi Xue](#)

The Chinese University of Hong Kong

4 PUBLICATIONS 16 CITATIONS

[SEE PROFILE](#)



[Ge Lin](#)

The Chinese University of Hong Kong

178 PUBLICATIONS 3,322 CITATIONS

[SEE PROFILE](#)

Proteomic Study of Pyrrolizidine Alkaloid-Induced Hepatic Sinusoidal Obstruction Syndrome in Rats

Yan-Hong Li,^{†,‡,#} William Chi-Shing Tai,^{‡,§,#} Jun-Yi Xue,[†] Wing-Yan Wong,[‡] Cheng Lu,^{‡,||} Jian-Qing Ruan,[†] Na Li,[†] Tai-Fung Wan,[†] Wood-Yee Chan,[†] Wen-Luan Wendy Hsiao,^{*,‡,⊥} and Ge Lin^{*,†}

[†]School of Biomedical Sciences, Faculty of Medicine, The Chinese University of Hong Kong, Hong Kong, China

[‡]Centre of Cancer and Inflammation Research, School of Chinese Medicine, Hong Kong Baptist University, Hong Kong, China

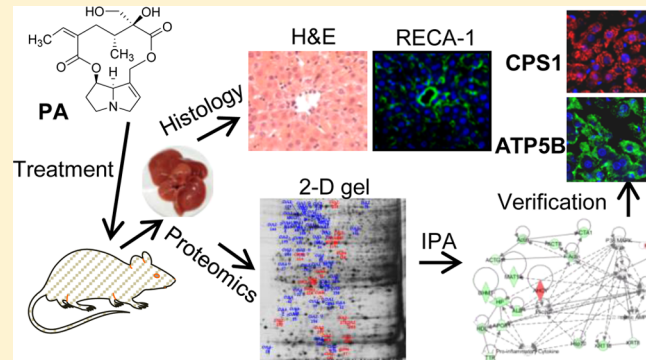
[§]Institute of Integrated Bioinfomedicine & Translational Science, Hong Kong Baptist University Shenzhen Research Institute and Continuing Education, Shenzhen, China

^{||}Institute of Basic Research in Clinical Medicine, China Academy of Chinese Medical Sciences, Beijing, China

[⊥]State Key Laboratory of Quality Research in Chinese Medicines, Macau University of Science and Technology, Macau, China

Supporting Information

ABSTRACT: Pyrrolizidine alkaloids (PAs) are a group of phytotoxins that can induce human liver injury, particularly hepatic sinusoidal obstruction syndrome (HSOS). To date, the molecular targets of PA-induced HSOS are largely unknown. In this study, retrorsine (RTS), a known hepatotoxic PA, was used as a representative PA for proteomic studies. Toxicological assessment demonstrated that 35 mg/kg RTS (designated as RTS-L) caused early lesions of HSOS at 24 h after dosing. A proteomic approach revealed 17 up-regulated and 31 down-regulated proteins in RTS-L-treated rats. Subsequently, bioinformatic analysis suggested that two proteins, carbamoyl-phosphate synthase (CPS1) ($p < 0.05$) and ATP synthase subunit beta (ATPSB) ($p < 0.01$) were associated with RTS-L intoxication. Using immunohistochemical staining, we further verified the down-regulation of CPS1 and ATPSB in RTS-L-treated rats. These findings indicated that CPS1 and ATPSB were altered in the RTS-induced early lesions of HSOS in rats, and therefore, these two proteins and their involved pathways might play important roles in the initiation of HSOS. To the best of our knowledge, our study using a proteomic approach combined with conventional toxicological assessment is the first systems toxicology study on PA-induced HSOS. The results of this study provide novel findings on protein profiles in response to PA exposure, which can serve as a starting point to further investigate potential protein targets and their interactions with PAs to induce HSOS.



INTRODUCTION

Pyrrolizidine alkaloids (PAs) are naturally occurring phytotoxins.¹ To date, more than 660 PAs and their N-oxides have been identified in over 6,000 plant species, which account for about 3% of the world's flowering plants.^{2,3} Among identified PAs, more than half have been reported to exhibit hepatotoxic activity. To date, since the first record of outbreak in 1920, numerous human PA poisoning cases have been reported.^{3–6} Apparently, PAs are likely one of the leading phytotoxins associated with human liver injury.

In humans, the intake of PA-containing products is a major cause of hepatic sinusoidal obstruction syndrome (HSOS).⁷ However, the mechanisms of HSOS are largely unknown, which limits the establishment of effective approaches for diagnosis and treatment.^{8,9} The current strategy to prevent PA-induced toxicity is to reduce and avoid PA exposure. Therefore, many countries and organizations have set regulations to restrict PA exposure.¹⁰ However, poisoning incidents con-

tinuously occur due to the intake of PA-contaminated foodstuffs and/or misuse of PA-containing herbs.^{6,11} There is thus an urgent need to uncover the mechanism underlying PA-induced toxicity.

PAs are generally divided into three types, based on different necine bases in the structures, namely, retronecine-, otonecine-, and platyphylline-types (Figure S1).^{12,13} Unsaturated PAs (retronecine- and otonecine-types) are hepatotoxic and metabolically activated by hepatic cytochrome P450 monooxygenases to form reactive metabolites, which rapidly react with cellular macromolecules, such as DNA and proteins in the liver, leading to toxicity.^{13–16} Studies *in vitro* have shown that these reactive PA metabolites directly damage sinusoidal endothelial cells (ECs), suggesting that ECs, but not parenchymal cells, are potentially the targets of toxicity in the

Received: March 17, 2015

liver.^{17,18} The depletion of glutathione (GSH), impaired NO production, and a default in the energy metabolism have been demonstrated to play roles in PA-induced toxicity.^{19–23} However, exactly how PAs act on ECs in the early stages, leading to HSOS, are unknown. Thus, studies applying advanced technologies to define the molecular mechanisms of PAs are required.

In recent years, “omic” technologies have been applied as promising tools for the elucidation of mechanisms of different toxins.^{23–25} In particular, proteomics, which has a unique capability to simultaneously identify and quantify a relatively large number of proteins, enables us to identify the responsible proteins. The resulting protein expression profiles may provide insights into the pathogenic processes of specific toxicities.^{26–28} Thus, the identification of altered proteins in the liver associated with PA toxicity may provide important information regarding its mechanism of toxicity.

To the best of our knowledge, to date only one proteomic study of PAs with a single dose in mice has been reported.²⁹ However, in that study, whether the induced toxicity reflects any pathogenesis of HSOS was not evaluated, and thus, how the observed proteomic responses relate to PA-associated HSOS remains unclear. It has been shown that the lesions of PA-induced toxicities are dose- and time-dependent.³⁰ Currently, little is known about what dosage/duration of PA exposure could induce HSOS. Therefore, in our present study we conducted, for the first time, a proteomic study of the early lesion of PA-induced hepatotoxicity combined with conventional toxicological assessments of different doses and exposure times of PA to evaluate the molecular events in a defined early stage of PA-induced HSOS.

MATERIALS AND METHODS

Chemicals. Retrorsine (RTS), cyclophosphamide (CP), sodium pyruvate, and GSH were purchased from Sigma-Aldrich Corporation (St. Louis, MO, USA). Primary antibodies were obtained from Abcam, Inc. (Cambridge, MA, USA). The solvents used in LC–MS/MS were of HPLC grade, and all other chemicals used were of analytical grade.

Animal Treatments. Male Sprague–Dawley rats, aged 12–15 weeks, were supplied by the Laboratory Animal Services Center at the Chinese University of Hong Kong. They were maintained on a 12-h light/dark daily cycle and in a controlled temperature (18–25 °C) and humidity (55 ± 5%) environment with food and water *ad libitum* for 3 days of acclimatization before experiments.

For toxicological assessments, rats were randomly divided into five groups ($n = 8$ per group except for the group with 35 mg/kg of RTS) and were administered by oral gavage with a single dose of vehicle (normal saline), RTS (dissolved in normal saline) at 35, 70, or 140 mg/kg, or CP (56 mg/kg), an agent known to induce HSOS at this dose.^{9,31–33} The three dosages of RTS (designated as RTS-L, RTS-M, and RTS-H) corresponded to 1-, 2-, and 4-fold of its median lethal dose (LD_{50}) in rats, respectively. The gavage volume for all groups was 1 mL/kg. The treated rats were fasted overnight and sacrificed 24 h after dosing. Liver samples of three randomly selected rats from the vehicle, RTS-L, and CP groups were used in proteomic studies. In the case of the 35 mg/kg RTS treatment group ($n = 11$), part of the animals ($n = 8$) were sacrificed at 24 h after dosing, while the rest of the animals ($n = 3$) were sacrificed at the third week after dosing, in order to examine whether HSOS developed in this extended observation period. In addition, a control group of rats ($n = 3$) receiving a single dose of vehicle (saline) was conducted in parallel.

The care and usage of animals were conducted with the license provided by the Department of Health, Government of Hong Kong SAR, and followed the guidelines approved by the Animal Ethics Committee of The Chinese University of Hong Kong.

Biochemistry and Histopathology. After treatment, rats were weighted and anesthetized with 20% urethane (5 mL/kg, ip). Serum was collected for the measurement of alanine transaminase (ALT) levels using a colorimetric end point method according to the manufacturer’s protocol.³⁴ Livers were weighed for relative liver weight (RLW) calculation [RLW = liver weight (LW)/body weight (BW) × 100%] and then subjected to a histological study.

Liver samples obtained from all treated rats were fixed in 4% buffered paraformaldehyde (PFA) and processed sequentially in ethanol, xylene, and paraffin. Tissues embedded in paraffin were sectioned (5 μm) and stained with hematoxylin and eosin (H&E). For immunohistochemical (IHC) staining, the freshly dissected livers of RTS-L, RTS-M, RTS-H, or CP-treated rats were fixed in 4% PFA, then cryoprotected in 30% sucrose solution. Tissues embedded in O.C.T. (Tissue-Tek O.C.T. compound) were cut into 5 μm thick slices and mounted onto positively charged microslides (Superfrost Plus slide, Menzel-Glaser). The sections were washed and blocked with 10% goat serum (VC-S-1000-L020, Vector laboratories, CA, USA) before incubation with mouse antirat endothelial cell (RECA-1) antibody (ab 9774, Abcam, Cambridge, MA, USA) (1:100 in blocking solution comprising 10% goat serum) overnight at 4 °C. Then they were washed and incubated with Alexa Fluor488 goat antimouse IgG (1:500; Invitrogen) for 1 h at room temperature in the dark. Finally, the sections were counterstained with DAPI-containing Permount (Fisher Scientific) and examined under a confocal microscope (Olympics Fluoview FV-1000) with a 40× objective lens.

For verification studies using IHC, the dilution of rabbit antirat CPS1 (ab45956, Abcam, Cambridge, MA, USA) and mouse antirat ATPSB (ab14748, Abcam, Cambridge, MA, USA) antibodies were 1:500 and 1:100, respectively. Images of stained sections were acquired with a Spot 1 camera using Spot 2.1 software (Diagnostic Instruments, Sterling Heights, MI). The gain was fixed for capturing all images after the determination of the highest possible gain setting without the introduction of noise. Adobe Photoshop CS3 software was used to quantify the intensities of CPS1 or ATPSB immunoreactive signals by normalizing to the signals of the vehicle control group. Briefly, the images were subjected to minimal color correction and corrected for chromatic aberration with the noise filter. For each image, three measuring fields of 200 × 200 pixels were randomly selected. A mean value of the histogram was assigned to each field by Adobe Photoshop CS3 software, and the average value of all three fields was used to assign a staining value (arbitrary units) to each image. A total of three randomly selected images from each of the three independent animals in each group were used in this quantification.

Two-Dimensional Gel Electrophoresis. Proteomic studies were performed on three rats per group at 24 h after a single dosing of RTS-L, 56 mg/kg CP, or vehicle control. Protein samples of individual rat liver tissues were extracted by homogenizing with 2D protein extraction buffer (9 M urea, 65 mM DTT, and 2% CHAPS) and then subjected to centrifugation at 100,000g for 1 h at 10 °C. The supernatants were collected, and protein concentration was determined by 2D Quant Kit (GE Healthcare, Fairfield, CT). Individual protein samples (120 μg) dissolved in 250 μL of rehydration buffer (8 M urea, 24% CHAPS, 2% DTT, 0.5% IPG ampholytes, and 1% bromophenol blue) were loaded on IPG strips (4–7 linear pH gradients, 13 cm length). IEF was then carried out in an Ettan IPGphor 3 IEF System (GE Healthcare) at 80,000 V/h. The resulting strips were equilibrated in SDS equilibration buffer (6 M urea, 75 mM Tris-HCl buffer, pH 8.8, 30% (v/v) glycerol, and 2% SDS) and then subjected to 12.5% SDS polyacrylamide gel separation. Protein spots were visualized in silver stain sensitizing solution. Reactions were stopped with 1.46% EDTA solution, and the gels were washed and stored in water.

Image Analysis and Spot Identification. The silver-stained gels were scanned at an optical resolution of 300 dpi on a gel scanner ImageScanner III (GE Healthcare). The digitized images were analyzed using Progenesis SameSpots software (Nonlinear Dynamics, Durham, NC, USA) according to protocols provided by the manufacturer. Spot intensities were quantified by calculation of spot volume after normalization of the image using the total spot volume

Table 1. Rat Body and Liver Weight before and after RTS and CP Treatment^a

group	BW (g) pretreatment	BW (g) post-treatment	net BW decrease (g)	LW (g) post-treatment	RLW (%) post treatment
vehicle	258 ± 8.0	236 ± 10.1	21.8 ± 3.3	7.5 ± 0.6	3.2 ± 0.3
RTS (mg/kg)	35	254 ± 8.3	232 ± 9.8	22.0 ± 3.0	3.4 ± 0.1
	70	248 ± 6.7	227 ± 5.8	20.4 ± 4.2	3.5 ± 0.1 ^b
	140	262 ± 9.2	240 ± 3.3	22.2 ± 3.9	3.7 ± 0.3 ^b
CP (56 mg/kg)	254 ± 8.6	235 ± 10.1	18.8 ± 3.6	8.2 ± 0.2 ^b	3.5 ± 0.1 ^b

^aBW, body weight; LW, liver weight; RLW, relative liver weight = LW/BW × 100%. Data are presented as the mean ± SD ($n = 8$). ^b $p < 0.05$ compared to the vehicle control.

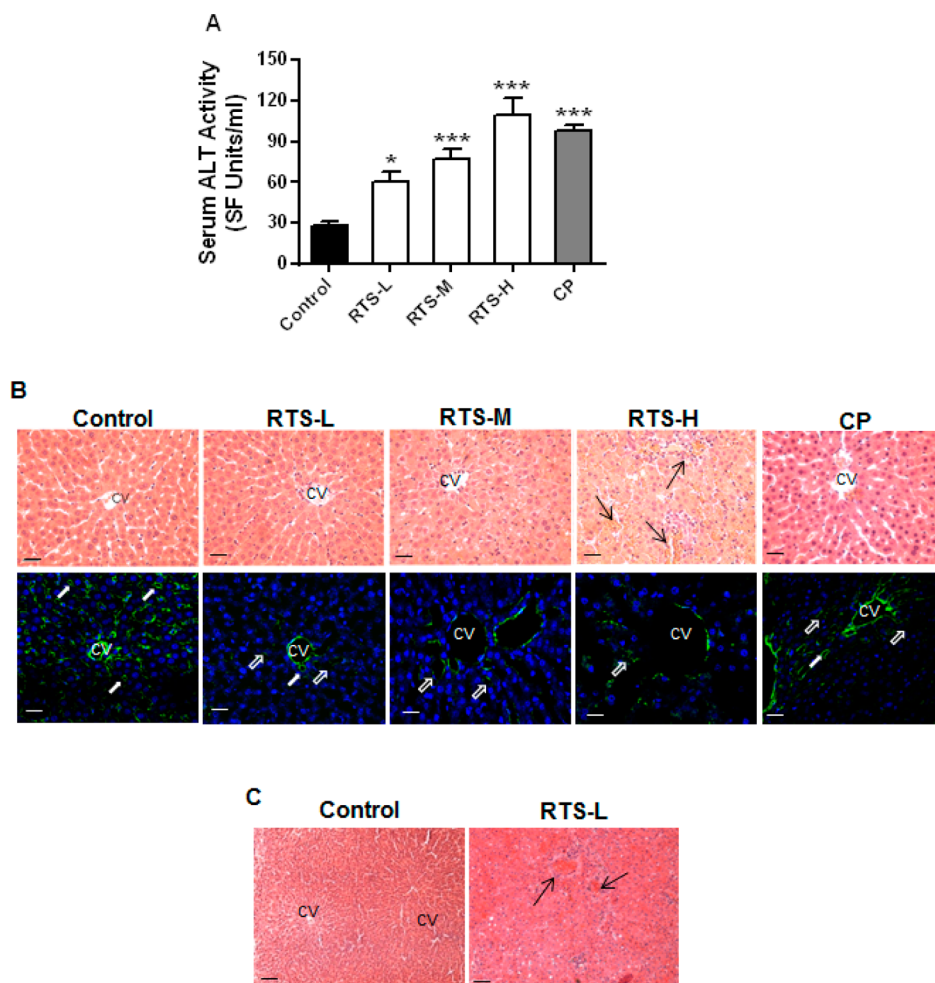


Figure 1. Hepatotoxicity of RTS and CP in rats. (A) Effect of 35, 70, and 140 mg/kg RTS (designated as RTS-L, RTS-M, and RTS-H), and 56 mg/kg CP treatment ($n = 8$). * $p < 0.05$ and *** $p < 0.001$ compared to the vehicle control group. (B) Histological analysis of liver damage caused by three doses of RTS and 56 mg/kg CP ($n = 8$). H&E staining (top row) reveals obvious liver injury including dilation of the sinusoid and hemorrhage (→), occlusion of the central vein (CV), and lobule disarray. IHC staining (bottom row) showed the endothelial cell (EC) lining on CVs and sinusoids. ECs were immunostained with antiendothelial cell antibody (RECA-1) in green color, while nuclei were stained with DAPI in blue color. Normal and injured sinusoids are indicated by “closed arrows” and “open arrows”, respectively. Scale bar = 25 μ m. (C) H&E staining shows sinusoidal obstruction (→) at the third week after a single dose of RTS-L treatment ($n = 3$). Scale bar = 50 μ m.

normalization method multiplied by the total area of all the spots. The 2-DE images from treatment groups were each compared with the control using the SameSpots software. The p -values were calculated by the software using ANOVA. Protein spots showing a quantitative difference of + or -1.2-fold changes with a p -value <0.05 indicating significant changes were selected for subsequent protein identification.

Protein Identification. For protein identification, individual protein spots of interest were excised from gels, destained, and dehydrated before being subjected to trypsin (Promega, Madison, WI) digestion. Peptides were then extracted, vacuum-dried, and stored at -20 °C prior to mass spectrometry (MS) analysis. Proteins were identified using an Autoflex III MALDI TOF/TOF MS (Bruker,

Germany) equipped with a 200 Hz N2 laser ($\lambda = 337$ nm). Data were acquired in the positive ion reflector mode over a mass range of 800–4000 Da. External calibration was performed using peptide calibration standards (Bruker Daltonics). Keratin contamination peaks, matrix ion peaks, and trypsin ion peaks were excluded from spectra. Typically, 400 shots were accumulated per spectrum in MS mode and 2,000 shots in MS/MS mode. All spectra were processed using FlexAnalysis 3.0 and BioTools 3.1 software tools (Bruker, Germany). The peptide mass fingerprinting was compared with the International Protein Index (IPI) database using the Mascot search program (version 2.2.04, <http://www.matrixscience.com>) to identify the corresponding proteins. Parameters for database searches were as follows: monoisotopic

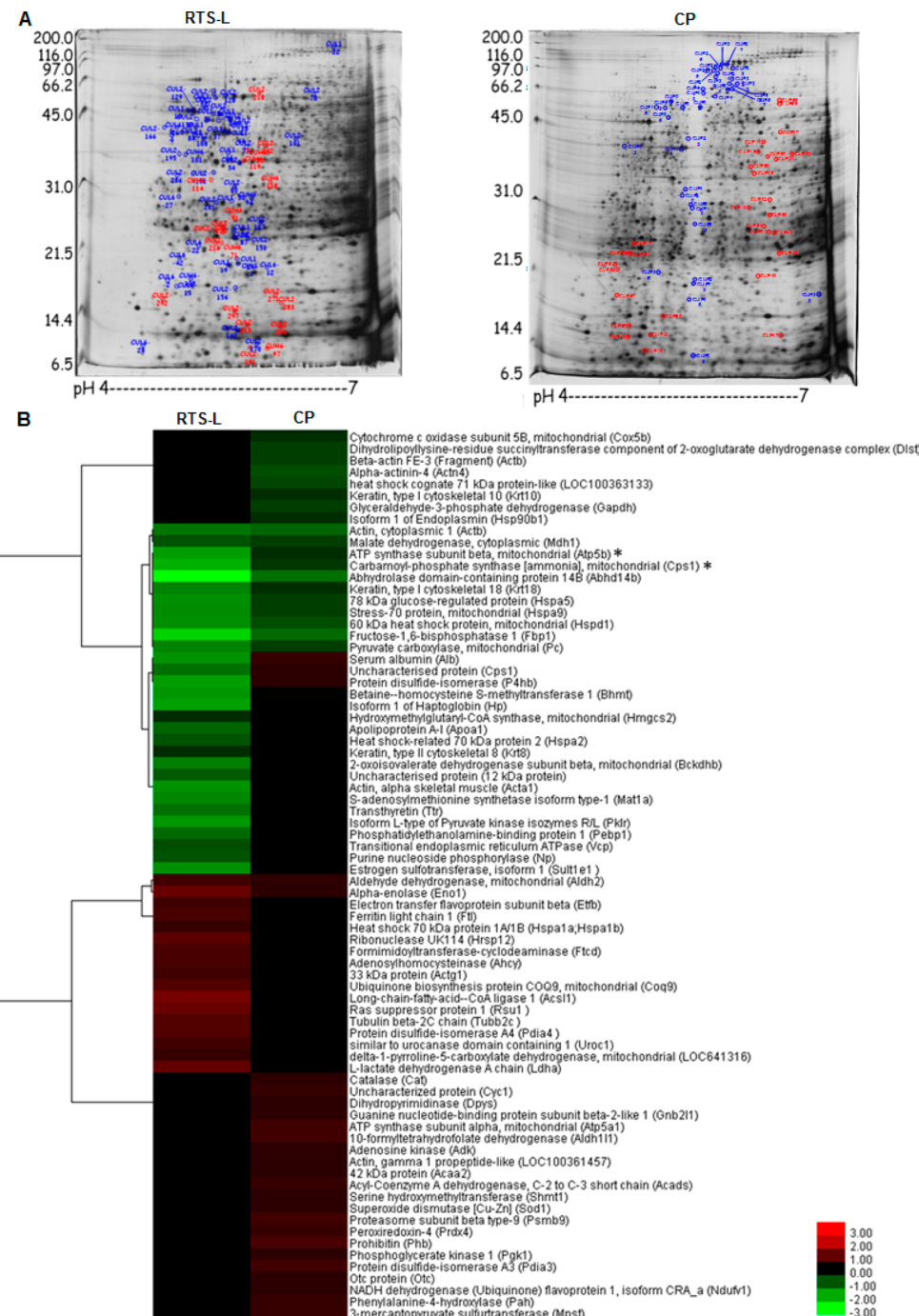


Figure 2. (A) Representative 2-D gel of proteins in the liver obtained from rats at 24 h after RTS-L and 56 mg/kg CP treatments ($n = 3$). Significantly changed protein dots were circled and indicated with respective ID codes. Red, up-regulated; blue, down-regulated compared to the vehicle control. (B) The representative clustered display of 79 differentially expressed proteins obtained from both RTS-L and CP-treatment groups, compared with the vehicle control. Red indicates up-regulated and green indicates down-regulated proteins.

mass accuracy <100 ppm; missed cleavages up to 1; carbamido methylation of cysteine as fixed modification; and the oxidation of methionine as variable modifications. In MS/MS mode, the fragment ion mass accuracy was set to <0.5 Da.

Hierarchical Clustering Analysis. Hierarchical clustering of protein expression patterns was performed using Cluster software version 3.0. The standard statistical algorithm of the average-linkage method was selected to arrange fold changes of identified proteins according to their similarity metrics.³⁵ This algorithm was used to construct a dendrogram that assembled all elements into a single tree. All the other parameters in the software were set as default, and the

hierarchical clustering results were visualized by TreeView software (version 1.1.4, <http://rana.lbl.gov/downloads/TreeView/>).³⁵

Bioinformatics Analysis. All differentially expressed proteins of both treated groups were uploaded and mapped to the library of canonical pathways of the IPA database for pathway analysis (Ingenuity Systems, version 3.77, <http://www.ingenuity.com>, Mountain View, CA). The mapped data sets containing either up-regulated or down-regulated protein in liver samples from different treatment groups with corresponding expression values were subjected to “core” and “comparison” analyses that included overall canonical pathway enrichment analysis. Further, network construction was performed by

Table 2. Hepatic Differentially Expressed Proteins Identified by MALDI-TOF/TOF at 24 h of Treatment of 35 mg/kg RTS and 56 mg/kg CP^a

no.	protein ID	description	RTS-L treatment			accession no.	Mascot score	no. of matched peptides	sequence coverage (%)
			fold change	p value	q value				
L1	Acsl1	long-chain-fatty-acid-CoA ligase 1	+2.3	0.0001	0.1088	IPI00188989	185	5	5
L2	eno1	alpha-enolase	+2.1	0.0100	0.1890	IPI00464815	496	7	23
L3	Rsu1	Ras suppressor protein 1	+2.1	0.0200	0.2325	IPI00364932	163	2	9
L4	Ldha	L-lactate dehydrogenase A chain	+2.0	0.0050	0.1597	IPI00197711	103	2	5
L5	Hrsp12	ribonuclease UK114	+1.9	0.0070	0.1502	IPI00231292	248	2	18
L6	Pdia4	protein disulfide-isomerase A4	+1.8	0.0060	0.1597	IPI00212220	76	3	2
L7	Tubb2c	tubulin beta-2C chain	+1.8	0.0230	0.2431	IPI00400573	602	18	28
L8	Coq9	ubiquinone biosynthesis protein COQ9, mitochondrial	+1.8	0.0310	0.2431	IPI00365149	264	4	17
L9	Ahcy	adenosylhomocysteine	+1.7	0.0400	0.2463	IPI00476295	163	3	7
L10	Ftl	ferritin light chain 1	+1.7	0.0400	0.2463	IPI00679203	278	5	39
L11	Ftcd	formimidoyltransferase-cyclodeaminase	+1.7	0.0340	0.2316	IPI00211392	60	2	4
L12	Actg1	33 kDa protein	+1.6	0.0150	0.1957	IPI00948496	565	4	20
L13	Aldh2	aldehyde dehydrogenase, mitochondrial	+1.6	0.0130	0.1805	IPI00197770	238	5	11
L14	Etfb	electron transfer flavoprotein subunit beta	+1.6	0.0260	0.2293	IPI00364321	169	4	17
L15	Uroc1	similar to urocanase domain containing 1	+1.6	0.0060	0.1470	IPI00388707	75	1	1
L16	LOC641316	delta-1-pyrroline-5-carboxylate dehydrogenase, mitochondrial	+1.5	0.0130	0.1800	IPI00921682	122	2	5
L17	Hspa1a;Hspa1b	heat shock 70 kDa protein 1A/1B	+1.5	0.0290	0.2306	IPI00196751	33	1	2
L18	Abhd14b	abhydrolase domain-containing protein 14B	-9.1	0.0100	0.1658	IPI00188359	177	3	15
L19	Fbp1	fructose-1,6-bisphosphatase 1	-5.5	0.0330	0.2453	IPI00231745	233	4	9
L20	Cps1	carbamoyl-phosphate synthase [ammonia], mitochondrial	-4.2	0.0420	0.2463	IPI00210644	100	2	1
L21	Hp	isoform 1 of Haptoglobin	-3.7	0.0430	0.2547	IPI00565708	157	2	6
L22	Atp5b	ATP synthase subunit beta, mitochondrial	-3.6	0.0080	0.1540	IPI00551812	624	9	27
L23	P4hb	protein disulfide-isomerase	-3.6	0.0340	0.0338	IPI00198887	123	1	3
L24	Bhmt	betaine-homocysteine S-methyltransferase 1	-3.4	0.0230	0.2244	IPI00332027	56	1	2
L25	Pkrl	isoform L-type of pyruvate kinase isozymes R/L	-3.4	0.0020	0.1326	IPI00231683	325	9	20
L26	Acta1	actin, alpha skeletal muscle	-3.3	0.0090	0.1616	IPI00189813	49	1	2
L27	Alb	serum albumin	-3.3	0.0190	0.2254	IPI00191737	257	4	8
L28	Hspd1	60 kDa heat shock protein, mitochondrial	-3.2	0.0020	0.1282	IPI00339148	144	2	6
L29	Hspa5	78 kDa glucose-regulated protein	-3.2	0.0040	0.1511	IPI00206624	259	5	8
L30	Sult1e1	sult1e1 estrogen sulfotransferase, isoform 1	-3.2	0.0100	0.1890	IPI00198376	91	2	6
L31	Hspa9	stress-70 protein, mitochondrial	-3.1	0.0040	0.1407	IPI00363265	186	5	9
L32	Mat1a	S-adenosylmethionine synthetase isoform type-1	-3.0	0.0090	0.1579	IPI00201436	279	4	15
L33	Krt18	keratin, type I cytoskeletal 18	-2.9	0.0170	0.1980	IPI00480679	209	6	15
L34	Pc	pyruvate carboxylase, mitochondrial	-2.9	0.0360	0.2356	IPI00210435	211	6	6
L35	Bckdhb	2-oxoisovalerate dehydrogenase subunit beta, mitochondrial	-2.8	0.0010	0.1088	IPI00201636	66	1	2
L36	Actb	actin, cytoplasmic 1	-2.6	0.0100	0.1758	IPI00189819	239	7	21
L37	Ttr	transthyretin	-2.5	0.0170	0.1980	IPI00324380	192	2	25
L38	Cps1	uncharacterized protein	-2.5	0.0005	0.1174	IPI00950946	211	4	2
L39	Pebp1	phosphatidylethanolamine-binding protein 1	-2.4	0.0090	0.1605	IPI00230937	146	2	11
L40	Apoa1	apolipoprotein A-I	-2.3	0.0330	0.2316	IPI00197703	144	5	18
L41	12 kDa protein	uncharacterized protein	-2.1	0.0430	0.2463	IPI00189038	68	1	17
L42	Actg1	Actg1 33 kDa protein	-2.0	0.0440	0.2587	IPI00948496	153	3	15
L43	Hspa2	heat shock-related 70 kDa protein 2	-2.0	0.0007	0.1088	IPI00207355	50	1	1
L44	Mdh1	malate dehydrogenase, cytoplasmic	-2.0	0.0230	0.2244	IPI00198717	57	1	3
L45	Np	purine nucleoside phosphorylase	-2.0	0.0330	0.2316	IPI00870631	304	8	27
L46	Vcp	translational endoplasmic reticulum ATPase	-1.9	0.0380	0.2487	IPI00212014	141	3	2

Table 2. continued

no.	protein ID	description	RTS-L treatment				Mascot score	no. of matched peptides	sequence coverage (%)
			fold change	p value	q value	accession no.			
L47	Hmgcs2	hydroxymethylglutaryl-CoA synthase, mitochondrial	-1.5	0.0410	0.2463	IPI00210444	327	10	18
L48	Krt8	keratin, type II cytoskeletal 8	-1.5	0.0430	0.2471	IPI00389571	117	4	8
CP treatment									
no.	protein ID	description	fold change	p value	q value	accession no.	Mascot score	no. of matched peptides	sequence coverage (%)
P1	Phb	prohibitin	+1.7	0.0003	0.0924	IPI00211756	111	4	20
P2	Aldh1l1	10-formyltetrahydrofolate dehydrogenase	+1.6	0.0001	0.0591	IPI00196725	329	14	15
P3	Atp5a1	ATP synthase subunit alpha, mitochondrial	+1.6	0.0010	0.0924	IPI00396910	186	4	10
P4	Psmb9	proteasome subunit beta-type-9	+1.6	0.0480	0.2096	IPI00196819	109	10	47
P5	Pdia3	protein disulfide-isomerase A3	+1.6	0.0440	0.2012	IPI00324741	156	6	14
P6	Mpst	3-mercaptopyruvate sulfurtransferase	+1.5	0.0300	0.1920	IPI00231106	107	4	14
P7	Acads	acyl-coenzyme A dehydrogenase, C-2 to C-3 short chain	+1.5	0.0090	0.1554	IPI00231359	604	11	29
P8	Prdx4	peroxiredoxin-4	+1.5	0.0210	0.1729	IPI00208209	231	3	35
P9	Pah	phenylalanine-4-hydroxylase	+1.5	0.0450	0.2024	IPI00193258	331	11	20
P10	Alb	serum albumin	+1.5	0.0330	0.1933	IPI00191737	241	9	16
P11	Cyc1	uncharacterized protein	+1.5	0.0210	0.1699	IPI00366416	113	3	12
P12	Acaa2	42 kDa protein	+1.4	0.0070	0.1518	IPI00948721	233	9	28
P13	LOC100361457	actin, gamma 1 propeptide-like	+1.4	0.0170	0.1631	IPI00960003	166	5	19
P14	Adk	adenosine kinase	+1.4	0.0270	0.1920	IPI00214456	66	4	8
P15	Aldh2	aldehyde dehydrogenase, mitochondrial	+1.4	0.0030	0.1280	IPI00197770	552	11	24
P16	Eno1	alpha-enolase	+1.4	0.0080	0.1529	IPI00464815	118	4	12
P17	Cat	catalase	+1.4	0.0200	0.1671	IPI00231742	240	7	18
P18	Dpys	dihydropyrimidinase	+1.4	0.0070	0.1506	IPI00205906	199	4	13
P19	Gnb2l1	guanine nucleotide-binding protein subunit beta-2-like 1	+1.4	0.0280	0.1920	IPI00231134	95	5	17
P20	Ndufv1	NADH dehydrogenase (ubiquinone) flavoprotein 1, isoform CRA_a	+1.4	0.0290	0.1920	IPI00191913	252	6	14
P21	Otc	Otc protein	+1.4	0.0340	0.1956	IPI00950491	340	9	23
P22	Pgk1	phosphoglycerate kinase 1	+1.4	0.0150	0.1631	IPI00231426	55	1	3
P23	P4hb	protein disulfide-isomerase	+1.4	0.0030	0.1280	IPI00198887	67	4	8
P24	Shmt1	serine hydroxymethyltransferase	+1.4	0.0330	0.1933	IPI00421364	226	5	9
P25	Sod1	superoxide dismutase [Cu-Zn]	+1.4	0.0180	0.1631	IPI00231643	224	2	17
P26	Cps1	uncharacterized protein	+1.4	0.0090	0.1554	IPI00950946	96	7	6
P27	Abhd14b	abhydrolase domain-containing protein 14B	-2.5	0.0120	0.1554	IPI00188359	98	4	21
P28	Fbp1	fructose-1,6-bisphosphatase 1	-2.4	0.0310	0.1920	IPI00231745	540	11	25
P29	Actb	actin, cytoplasmic 1	-2.3	0.0100	0.1554	IPI00189819	177	5	20
P30	Hspd1	60 kDa heat shock protein, mitochondrial	-1.9	0.0140	0.1612	IPI00339148	138	3	8
P31	Actn4	alpha-actinin-4	-1.9	0.0080	0.1529	IPI00213463	193	9	11
P32	LOC100363133	heat shock cognate 71 kDa protein-like	-1.8	0.0050	0.1441	IPI00959289	167	8	14
P33	Hspa5	78 kDa glucose-regulated protein	-1.7	0.0110	0.1554	IPI00206624	351	20	34
P34	Actb	beta-actin FE-3 (fragment)	-1.7	0.0320	0.1921	IPI00960010	177	2	21
P35	Dlst	dihydrolipoyllysine-residue succinyltransferase component of 2-oxoglutarate dehydrogenase complex	-1.7	0.0170	0.1631	IPI00551702	175	10	17
P36	Gapdh	glyceraldehyde-3-phosphate dehydrogenase	-1.7	0.0050	0.1441	IPI00554039	128	3	11
P37	Mdh1	malate dehydrogenase, cytoplasmic	-1.7	0.0190	0.1655	IPI00198717	124	2	6
P38	Pc	pyruvate carboxylase, mitochondrial	-1.7	0.0090	0.1554	IPI00210435	262	16	14
P39	Hspa9	stress-70 protein, mitochondrial	-1.7	0.0370	0.2007	IPI00363265	198	9	14
P40	Cps1	carbamoyl-phosphate synthase [ammonia], mitochondrial	-1.6	0.0460	0.2057	IPI00210644	337	22	11
P41	Atp5b	ATP synthase subunit beta, mitochondrial	-1.5	0.0140	0.1612	IPI00551812	109	7	18
P42	Cox5b	cytochrome c oxidase subunit 5B, mitochondrial	-1.5	0.0330	0.1921	IPI00193918	184	7	48
P43	Hsp90b1	isoform 1 of endoplasmic	-1.5	0.0020	0.1198	IPI00365985	225	7	10
P44	Krt18	keratin, type I cytoskeletal 18	-1.5	0.0410	0.2012	IPI00480679	157	6	16

^aFold change means the differentially up-regulated (+) or down-regulated (-) proteins in the treatment groups in comparison with the vehicle control group.

uploading protein IDs (IPI number) and quantitative data into IPA to discover the biological relationships between these proteins.³⁶

Statistical Analysis. All data are represented as the mean \pm SEM unless otherwise stated. In the toxicity study, for the comparison of different treatment groups, the data were analyzed by one-way ANOVA coupled with Dunnett's post-test using GraphPad Prism 5.0. $p < 0.05$ was considered statistically significant.

RESULTS

Characterization of RTS-Induced HSOS in Rats. To define the characteristic pattern of PA-induced HSOS, hepatotoxicity induced by RTS was monitored in the treated rats. At 24 h after a single oral administration of RTS-L, -M, and -H corresponding to 1-, 2-, or 4-folds of its LD₅₀, no fatality and no significant difference in body weight decrease were observed among all groups (Table 1). However, liver weight and relative liver weight were increased in a dosage dependent manner starting from the dose of 70 mg/kg, indicating the development of hepatomegaly after RTS-M treatment. Furthermore, serum ALT activity level was significantly elevated in all RTS treated groups (Figure 1A).

Obvious liver damages demonstrated by the dilation of sinusoids, destruction of CVs, and/or lobule disarray were observed in rats treated with RTS-M and RT-H, but not with RTS-L (Figure 1B, H&E staining). However, damage to sinusoidal ECs, which is characteristic of HSOS, was clearly demonstrated by the decreased intensity of RECA-1 immunofluorescence in the luminal surface of sinusoids in all RTS treated animals (Figure 1B, IHC staining). Lesions caused by CP treatment were closely comparable to those caused by RTS-L treatment (Figure 1A and B). The results indicated that RTS-L treatment induced early lesions with obvious damage in sinusoidal ECs only, while higher dosage of RTS caused more severe damage to sinusoidal ECs, to parenchymal cells, and then the entire liver.

To examine whether HSOS developed after a single dose of RTS-L treatment, an extended three-week observation period was adopted. Histological examination showed severe liver injury with complete occlusion of sinusoids and CVs as well as the disarray of the liver lobule (Figure 1C). This suggested that a single low dosage of RTS could cause an initial sinusoidal EC damage as early as 24 h and subsequently trigger an onset of a full-bloom of HSOS within 3 weeks.

Liver Protein Profiling of RTS-L-Treated Rats. Therefore, to delineate the protein expression changes in rat liver with early lesions of HSOS in response to PA exposure, proteomic studies were conducted more appropriately on the livers obtained from rats treated with RTS-L, and the results were compared with CP-treated rats. Liver proteins obtained from the control, RTS-, and CP-treated rats were extracted and separated by 2-DE (2D gel images in triplicate are shown in Figure S2).

In the RTS-L-treated group, 48 differentially expressed proteins were identified, with 17 up-regulated and 31 down-regulated, while CP treatment induced up-regulation of 26 proteins and down-regulation of 18 proteins (Figure 2A and Table 2). For further comparison, a dendrogram was used to illustrate the hierarchical clustering of the 79 identified proteins. As shown in Figure 2B, the results demonstrated that some altered proteins were consistently regulated by both RTS-L and CP, which implied that pathways involving these universally changed proteins might play roles in the pathogenesis of HSOS induced by both RTS and CP.

Bioinformatics Analysis Using IPA. To explore the biological networks involved in RTS-L-induced liver toxicity in the early stage, bioinformatics analysis was conducted using IPA software. Results revealed that the top scoring functional networks in the RTS-L-treated group were "cellular growth and proliferation, hematological disease, and immunological disease" and "lipid metabolism, molecular transport, and small molecular biochemistry;" while in the CP treatment group, they were "hematological disease, immunological disease, and inflammatory disease" and "nucleic acid metabolism, small molecular biochemistry, cellular growth, and proliferation" (Table 3).

Table 3. Top-Score Protein Networks Nominated by IPA Analysis

ID	associated network functions	score ^a
Top Networks of RTS treatment		
1	cellular growth and proliferation, hematological disease, immunological disease	55
2	lipid metabolism, molecular transport, small molecular biochemistry	23
3	developmental disorder, hematological disease, hereditary disorder	2
4	developmental disorder, hereditary disorder, metabolic disease	2
5	cancer, cell-to-cell signaling and interaction, nervous system development and function	2
Top Networks of CP Treatment		
1	hematological disease, immunological disease, inflammatory disease	59
2	nucleic acid metabolism, small molecular biochemistry, cellular growth and proliferation	37
3	amino acid metabolism, small molecular biochemistry, vitamin and mineral metabolism	2
4	drug metabolism, endocrine system development and function, lipid metabolism	2

^aThe network score is a numerical value used to rank networks according to their degrees of relevance to the network eligible molecules in the protein list.

In addition, IPA network analysis suggested that two proteins CPS1 and ATPSB were important and were presented in both RTS-L and CP treatment networks as shown in Figure 3. Moreover, the functions of these constructed networks also involved energy metabolism, mitochondrial dysfunction, inflammation response, and cell-to-cell signaling and interaction, which are similar to those as revealed by the above-mentioned top scoring functional network analysis (Table 3). These findings form a starting point for a rational hypothesis that both CPS1 and ATPSB could be potential protein targets and that the pathways involved could play important roles in the toxicity of RTS and CP.

Verification of Altered Expressions of CPS1 and ATP5B. Using a proteomic approach, CPS1 and ATP5B were found to be down-regulated in both RTS-L- and CP-treated rat livers (Figure 4). The altered expressions of hepatic CPS1 ($p < 0.05$; $q = 0.2463$) and ATP5B ($p < 0.01$; $q = 0.1540$) were then verified by IHC. The results showed that in the control group, CPS1 and APTSB signals were strongly expressed in the cytoplasm of liver cells, while in the RTS-L and CP-treated rats, the expression levels of CPS1 and ATP5B were significantly decreased (Figure 5), which are consistent with the results obtained from the proteomic study. Further IHC staining on liver sections obtained from RTS-M and RTS-H treatment groups revealed that both proteins were down-

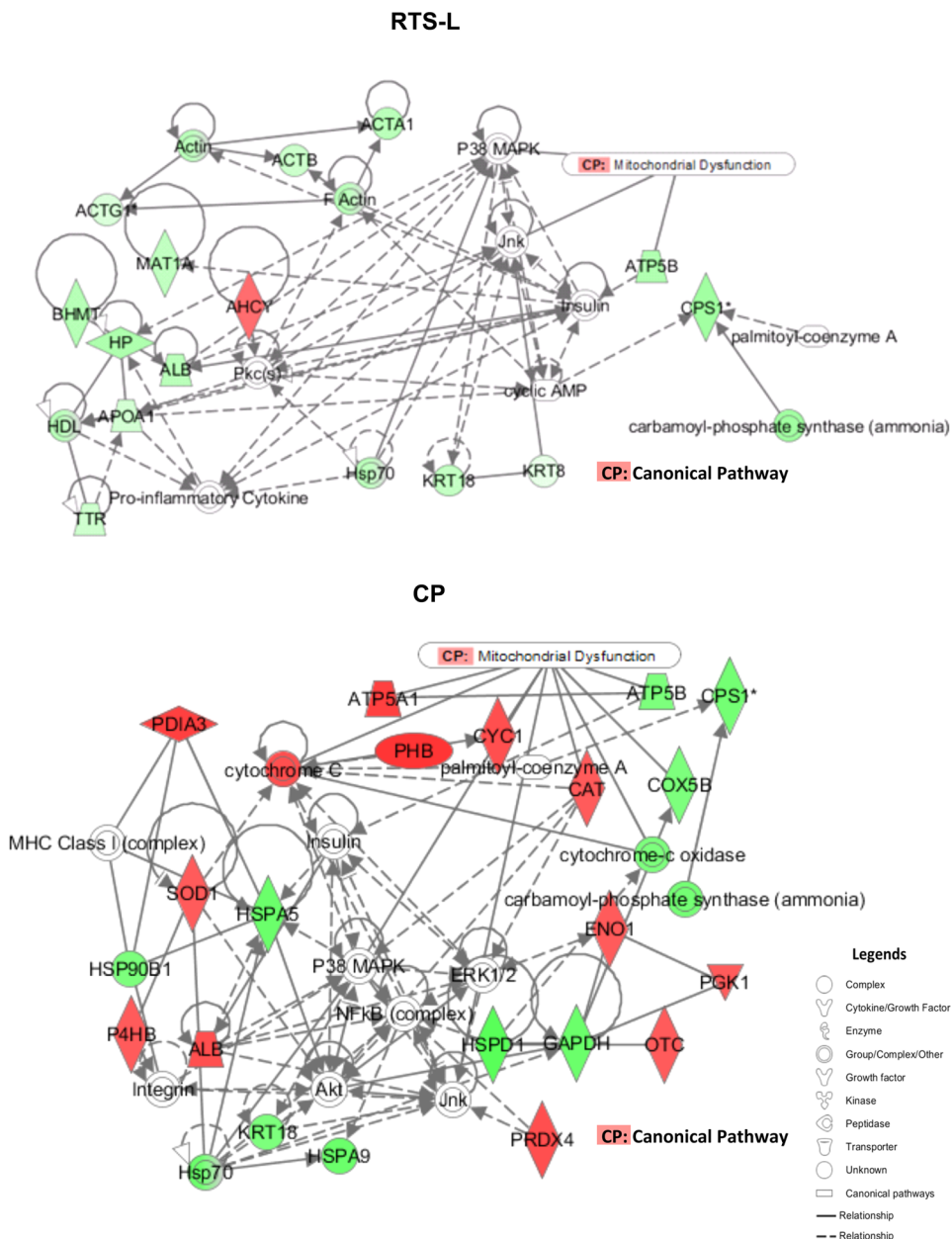


Figure 3. Identification of CPS1 and ATP5B by IPA network analysis for RTS-L and CP treatments. The nodes represent the proteins, and the lines between the nodes indicate the biological relationships between the two corresponding proteins. Note that the colored symbols indicate the proteins found in our study, whereas the open symbols are proteins identified by Ingenuity Knowledge Database. Red symbols represent the up-regulated proteins, and green symbols represent the down-regulated proteins. Solid lines indicate a direct physical relationship between the molecules, and the dotted lines indicate indirect functional relationships.

regulated by RTS-M, while they were up-regulated by RTS-H treatment (Figure 5).

■ DISCUSSION

In the present work, we performed a proteomic study to explore the events that trigger hepatotoxicity after PA administration. Retronecine-type PA is the most abundant type of PAs in plants, and their toxicities have been extensively studied. The RTS used in our study is a common retronecine-type of PA and has been found present in at least nine species of *Senecio*.³⁷ Like the other retronecine-type PAs, RTS, via metabolic activation, induces a variety of toxic responses, including acute and chronic hepatotoxicity, mutagenicity, and DNA cross-linking in kidney epithelial cells.^{38–40} Significantly,

RTS has been found to show toxicity specifically in the liver,^{12,41} indicating RTS as a suitable representative for exploring the mechanism of PA-induced hepatotoxicity. In addition, high doses of the anticancer drug CP can also cause HSOS.^{9,31–33} Therefore, CP was studied in parallel as a comparison in the present work.

To characterize the early lesions of PA-induced HSOS, toxicological experiments were performed. The findings showed that a dose-dependent hepatotoxicity was induced, as demonstrated by increasing liver weight and serum ALT level. Histopathological changes showed that obvious parenchymal cell damage only occurred upon medium and high dosages, but not at low dosage of RTS treatment. However, damage to sinusoids as assessed by detachment of sinusoidal ECs was

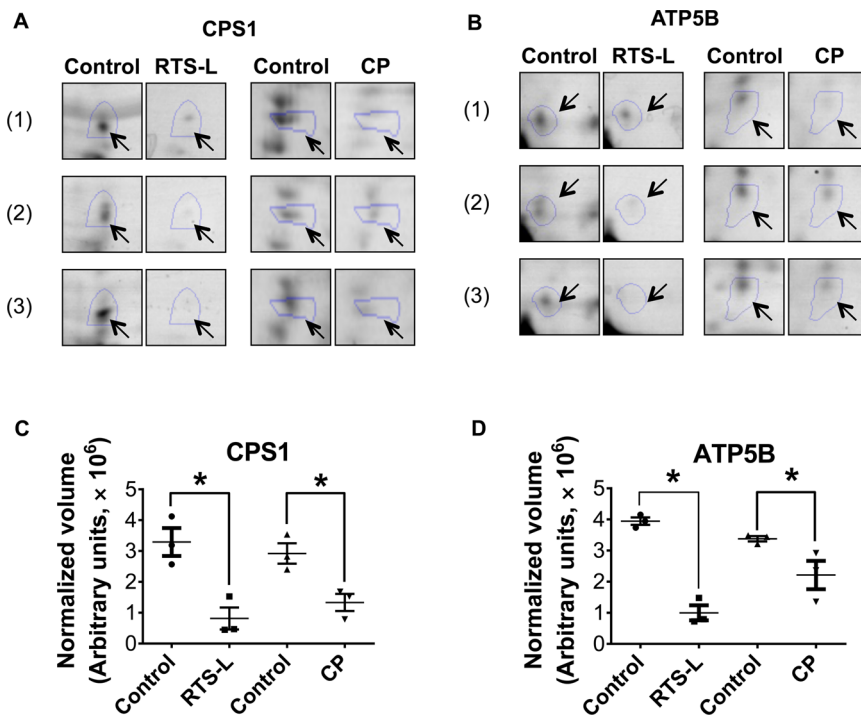


Figure 4. Down-regulation of CPS1 and ATP5B in the liver induced by RTS-L and CP, respectively revealed by proteomic analysis ($n = 3$). (A) Representative 2D-gel images of hepatic CPS1 expression. (B) Representative 2D-gel images of hepatic ATP5B expression. (C) Dotplots of normalized expression values of hepatic CPS1. (D) Dotplots of normalized expression values of hepatic ATP5B. * $p < 0.05$ comparing with the vehicle control group.

observed with RTS-L treatment. Moreover, development of HSOS was apparent in the rat liver at the third week after the treatment of a single dosage of RTS-L. These results indicated that a single dosing of RTS-L for 24 h triggered early onset of HSOS. While, the higher dosage of RTS and/or post-treatment time longer than 24 h could cause more severe liver injury in both sinusoidal ECs and parenchymal cells. Therefore, we adopted the protocol of RTS-L treatment for 24 h to further study the hepatic proteomic profiles in response to the early lesion of PA intoxication.

Using a quantitative proteomic approach, 48 differentially regulated proteins were identified after RTS-L treatment. Importantly, significant numbers of these identified proteins are involved in energy metabolism. For instance, CPS1 is involved in the urea cycle; ATP5B and malate dehydrogenase (MDH1) are in energy formation; S-adenosylmethionine synthetase isoform type-1 (MATLA) and betaine-homocysteine S-methyltransferase (BHMT) are involved in amino-acid biosynthesis; and isoform L-type of private kinase isozymes R/L (PKLR) is a rate limiting enzyme in the glycolysis pathway. It is of worth to note that in the study reported by Wong et al.,²⁹ 5 of the 13 differentially expressed proteins are also related to energy metabolism, although the individual proteins are different from our findings. These consistent observations may provide a molecular explanation to a previous finding by Mingatto et al., in which they demonstrate that PA impairs energy metabolism via inhibiting glycogenolysis activation and gluconeogenesis/ureogenesis.⁴² Further, a recent metabolomic study performed on PA-induced HSOS showed that the urine level of several intermediate products of the TCA cycle (citrate, succinate, and alpha-ketoglutarate) were decreased, indicating the strong association of the dysfunctions of energy metabolism with PA intoxication.²³ This hypothesis was partially corroborated by our present results showing altered expression of energy metabolism-related liver proteins. Energy metabolism plays a pivotal role in maintaining the normal function of cells, and the impairment of these processes can have a negative consequence on liver cells. Thus, the dysfunction of energy metabolism may be implicated at least partly in the hepatotoxicity of PA in animals. Additionally, the other three proteins involved in the stress response were also down-regulated. They were molecular chaperone stress-70 protein (HSPA9), 60 kDa heat shock protein (Hspd1), and 78 kDa glucose-regulated protein (HSPAS). Moreover, two proteins, namely, phosphatidylethanolamine-binding protein 1 (PEBP1) and type I cytoskeletal 18 (KRT18), involved in thrombosis formation were down-regulated.

Previous studies report that CPS1 and ATP5B are associated with liver toxicity.^{43–45} Our IPA analysis indicated that both proteins were present in RTS and CP networks. Moreover, using IHC staining, we successfully verified that CPS1 and ATP5B were consistently down-regulated by RTS and CP treatments. Because both PA and CP could induce HSOS and alter these two proteins, it is likely that CPS1 and ATP5B might play roles in the pathogenesis of HSOS. To further explore how CPS1 and ATP5B expressions correlate with different degrees of PA intoxication, we examined and compared their expressions in the livers of rats treated with different doses of RTS using IHC analysis (Figure 5). Interestingly, the expressions of both CPS1 and ATP5B were found decreased in RTS-L and RTS-M treatment groups, while they were increased in the RTS-H group. These observations suggest that the responses of CPS1 and ATP5B to different degrees of PA intoxication involve complex and dynamic events, in which their down-regulation may indicate a primary effect of sinusoidal EC losses in the early lesion of HSOS, while the

expressions of both CPS1 and ATP5B were found decreased in RTS-L and RTS-M treatment groups, while they were increased in the RTS-H group. These observations suggest that the responses of CPS1 and ATP5B to different degrees of PA intoxication involve complex and dynamic events, in which their down-regulation may indicate a primary effect of sinusoidal EC losses in the early lesion of HSOS, while the

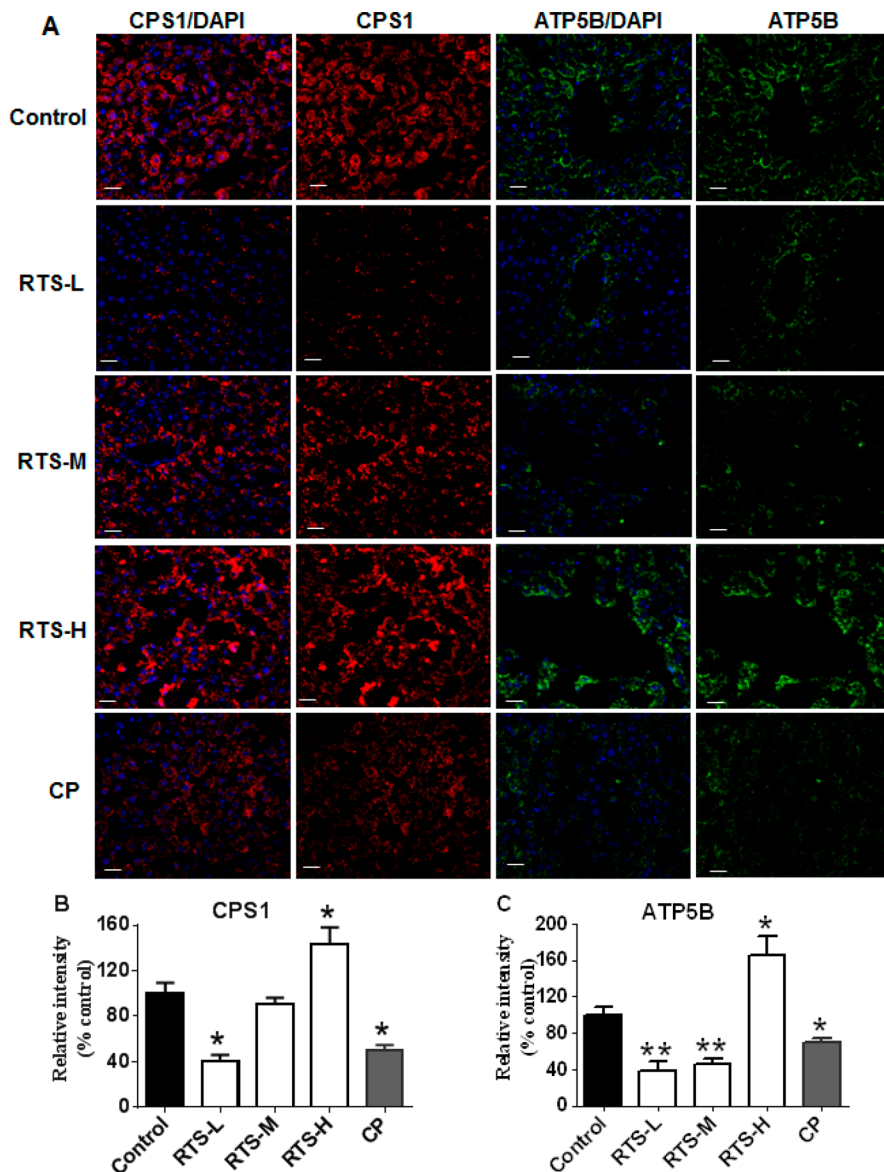


Figure 5. Verification of expression changes of CPS1 and ATPSB in the liver induced by RTS and CP. (A) IHC staining of hepatic CPS1 (red fluorescent) and ATPSB (green fluorescent). The merged figures are indicated as CPS1/DAPI and ATPSB/DAPI. Scale bar = 25 μ m. (B) Quantitative analysis of the IHC expression levels of CPS1. (C) Quantitative analysis of the IHC expression levels of ATPSB. * p < 0.05 and ** p < 0.01 compared with the vehicle control group.

up-regulation may be related to the subsequent further/secondary damages beyond sinusoidal ECs, such as the destruction of CV and lobule disarray as indicated in Figure 1B (RTS-H) and confirmed by double staining of CPS1 and RECA-1 in the RTS-H treatment (Figure S3). However, up to date no information was available on the functions of CPS1 and ATPSB and their pathways in PA intoxication and HSOS; therefore, future studies are warranted to delineate their role in HSOS.

CPS1 is the most abundant proteins in liver mitochondria, accounting for nearly 20% of the matrix protein mass and is the marker of the urea cycle.⁴⁴ In the mitochondrial matrix, CPS1 catalyzes the conversion of ammonia and bicarbonate into carbamoyl phosphate, which is the first and rate-limiting step in the urea cycle. The liver is the major site of conversion of amino-N to urea, and the urea cycle is the only nondietary source of essential substrates (arginine or citrulline) for endothelial NO synthesis and is well-known as the main

pathway for the removal of potential toxic ammonium from blood.^{46,47} Thus, the CPS1 decrease caused by PA revealed in our present study may explain why PA could cause NO decrease and inhibit ureogenesis as reported in previous studies.^{23,42} In addition, decreased levels of CPS1 harbor the possibility of lowering the function of the urea cycle, resulting in the accumulation of toxic ammonium in the circulation. Both NO decrease and ammonium accumulation may directly exert harmful effects on sinusoidal ECs. In addition, a subtoxic dose of PA has been reported to aggravate HSOS by inhibiting NO synthesis, and the decrease of NO production contributes to the development of HSOS in rats.⁴⁸ In addition, it has been found that impairment of both urea cycle function and NO production by intensive chemotherapy could predispose patients to oxidative organ injury and HSOS.⁴⁹ Therefore, it is rational to hypothesize that CPS1-regulated NO depletion via the urea cycle is vital for initiating lesions in sinusoidal ECs before the development of HSOS.

ATPSB is the major catalytic subunit of ATP synthase, which catalyzes the rate-limiting step of ATP production from ADP in the presence of a proton gradient across the mitochondrial membrane. Hence, ATPSB represents the key protein involved in the mitochondria dysfunction pathway, which was first described in the 1960s.^{50,51} However, its potential involvement in the pathogenesis of HSOS has not been reported. Several studies using *in vitro* models showed that PA and its metabolite impaired ATP production and mitochondrial energetics.^{52,53} In addition, the expression of hepatic ATPSB was also found to be significantly decreased upon ischemia/reperfusion injury,^{45,54} implying a pathogenesis similar to that of the involvement of hypoxic injury with RTS and CP exposure. Moreover, recent studies revealed that ATPSB was also present on the surface of vascular ECs.^{55,56} Angiostatin, a potent antagonist of angiogenesis and an inhibitor of EC migration and proliferation, has been shown to be able to bind with plasma membrane-localized ATPSB.⁵⁷ This binding was speculated to disrupt the production of ATP, rendering ECs more vulnerable to hypoxic challenge and eventual irreversible cell damage. Although it has not yet been shown, it is highly possible that ATPSB also locates on the surface of hepatic sinusoidal ECs. Therefore, the detected down-regulation of ATPSB in our study may partly originate from sinusoidal ECs, which could form an important factor to boost the damage to ECs.

CONCLUSIONS

Systems toxicology is a new concept using conventional toxicology combined with an “omic” approach to explore toxicity mechanisms.^{58,59} Our present study has generated a comprehensive systems toxicology analysis of the rat liver with early lesions of HSOS in response to PA for the first time. We demonstrated that the representative PA RTS had profound interactions with liver proteins. Two proteins, namely, CPS1 and ATPSB, were altered by RTS, and their involved pathways (urea cycle and mitochondria dysfunction) were thus suggested to play roles in the upstream damage of rat liver in HSOS formation. In summary, all of the findings extend our understanding of how PA causes hepatic lesions in the early stages of HSOS. The identified proteins and the aforementioned pathways provided rational hypotheses that warrant future validation by studying different PAs including toxic and nontoxic ones with different dosage regimens.

ASSOCIATED CONTENT

Supporting Information

The Supporting Information is available free of charge on the ACS Publications website at DOI: [10.1021/acs.chemrestox.5b00113](https://doi.org/10.1021/acs.chemrestox.5b00113).

Figure S1. Structure of three necine bases of PAs; Figure S2. Three representative 2D gel images of rat liver samples obtained from RTS-L treatment and the corresponding control group, and CP treatment and the corresponding control group; Figure S3. IHC double-staining of hepatic CPS1 (red fluorescent) and RECA-1 (green fluorescent). The merged figures are indicated as CPS1/RECA-1/DAPI.

(PDF)

AUTHOR INFORMATION

Corresponding Authors

*(W.-L.W.H.) Tel: +853 8897 2751. Fax: + 853 2882 5886. E-mail: wlhsiao@must.edu.mo.

*(G.L.) Tel: +852 3943 6824. Fax: +852 2603 5139. E-mail: linge@cuhk.edu.hk.

Author Contributions

#Y.-H.L. and W.-C.S.T. contributed equally to this work.

Funding

This work was supported by Research Grant Council of Hong Kong SAR (GRF Grants, Project Nos. 469712 and 471013), The Chinese University of Hong Kong (Direct Grants 4054134 and 4054215), and CUHK School of Biomedical Sciences—Seed Fund for Joint Establishments.

Notes

The authors declare no competing financial interest.

ACKNOWLEDGMENTS

We thank Dr. Martha Dahlen for editing this manuscript.

ABBREVIATIONS

ATPSB, ATP synthase subunit beta, mitochondrial; CP, cyclophosphamide; CPS1, carbamoyl-phosphate synthase [ammonia], mitochondrial; CV, central vein; ECs, endothelial cells; HSOS, hepatic sinusoidal obstruction syndrome; IHC, immunohistochemical; IPA, ingenuity pathways analysis; PA, pyrrolizidine alkaloid; RECA-1, antirat endothelial cell antibody; RTS, retrorsine

REFERENCES

- Smith, L. W., and Culvenor, C. C. (1981) Plant sources of hepatotoxic pyrrolizidine alkaloids. *J. Nat. Prod.* 44, 129–152.
- Roeder, E., and Wiedenfeld, H. (2011) Pyrrolizidine alkaloids in plants used in the traditional medicine of Madagascar and the Mascarene islands. *Pharmazie* 66, 637–647.
- Li, N., Xia, Q. S., Ruan, J. Q., Fu, P. P., and Lin, G. (2011) Hepatotoxicity and tumorigenicity induced by metabolic activation of pyrrolizidine alkaloids in herbs. *Curr. Drug Metab.* 12, 823–834.
- Bane, A., Seboxa, T., Mesfin, G., Ali, A., Tsegaye, Y. W., Tensae, M., Selassie, S. G., and Haile, T. (2012) An outbreak of veno-occlusive liver disease in northern Ethiopia, clinical findings. *Ethiop. Med. J.* 50 (Suppl 2), 9–16.
- Gao, H., Li, N., Wang, J. Y., Zhang, S. C., and Lin, G. (2012) Definitive diagnosis of hepatic sinusoidal obstruction syndrome induced by pyrrolizidine alkaloids. *J. Dig. Dis.* 13, 33–39.
- Lin, G., Wang, J. Y., Li, N., Li, M., Gao, H., Ji, Y., Zhang, F., Wang, H., Zhou, Y., Ye, Y., Xu, H. X., and Zheng, J. (2011) Hepatic sinusoidal obstruction syndrome associated with consumption of *Gynura segetum*. *J. Hepatol.* 54, 666–673.
- Chojkier, M. (2003) Hepatic sinusoidal-obstruction syndrome: toxicity of pyrrolizidine alkaloids. *J. Hepatol.* 39, 437–446.
- Winter, H., Seawright, A. A., Hrdlicka, J., Mattocks, A. R., Jukes, R., Wangdi, K., and Gurung, K. B. (1993) Pyrrolizidine alkaloid poisoning of yaks: diagnosis of sulphur-conjugated pyrrolizidine alkaloid exposure by the demonstration of sulphur-conjugated pyrrolizidine alkaloid metabolites of the alkaloid in circulating haemoglobin. *Aust. Vet. J.* 70, 312–313.
- Helmy, A. (2006) Review article: updates in the pathogenesis and therapy of hepatic sinusoidal obstruction syndrome. *Aliment. Pharmacol. Ther.* 23, 11–25.
- Cramer, L., Schiebel, H. M., Ernst, L., and Beuerle, T. (2013) Pyrrolizidine alkaloids in the food chain: development, validation, and application of a new HPLC-ESI-MS/MS sum parameter method. *J. Agric. Food Chem.* 61, 11382–11391.

- (11) Rasenack, R., Muller, C., Kleinschmidt, M., Rasenack, J., and Wiedenfeld, H. (2003) Veno-occlusive disease in a fetus caused by pyrrolizidine alkaloids of food origin. *Fetal. Diagn. Ther.* 18, 223–225.
- (12) Li, Y. H., Kan, W. L., Li, N., and Lin, G. (2013) Assessment of pyrrolizidine alkaloid-induced toxicity in an in vitro screening model. *J. Ethnopharmacol.* 150, 560–567.
- (13) Fu, P. P., Xia, Q., Lin, G., and Chou, M. W. (2004) Pyrrolizidine alkaloids—genotoxicity, metabolism enzymes, metabolic activation, and mechanisms. *Drug Metab. Rev.* 36, 1–55.
- (14) Yang, Y. C., Yan, J., Doerge, D. R., Chan, P. C., Fu, P. P., and Chou, M. W. (2001) Metabolic activation of the tumorigenic pyrrolizidine alkaloid, riddelliine, leading to DNA adduct formation in vivo. *Chem. Res. Toxicol.* 14, 101–109.
- (15) Ruan, J., Yang, M., Fu, P., Ye, Y., and Lin, G. (2014) Metabolic activation of pyrrolizidine alkaloids: insights into the structural and enzymatic basis. *Chem. Res. Toxicol.* 27, 1030–1039.
- (16) Ruan, J., Liao, C., Ye, Y., and Lin, G. (2014) Lack of metabolic activation and predominant formation of an excreted metabolite of nontoxic platynecine-type pyrrolizidine alkaloids. *Chem. Res. Toxicol.* 27, 7–16.
- (17) Copple, B. L., Banes, A., Ganey, P. E., and Roth, R. A. (2002) Endothelial cell injury and fibrin deposition in rat liver after monocrotaline exposure. *Toxicol. Sci.* 65, 309–318.
- (18) Copple, B. L., Rondelli, C. M., Maddox, J. F., Hoglen, N. C., Ganey, P. E., and Roth, R. A. (2004) Modes of cell death in rat liver after monocrotaline exposure. *Toxicol. Sci.* 77, 172–182.
- (19) Yan, C. C., and Huxtable, R. J. (1995) Effects of the pyrrolizidine alkaloid, retrorsine, on sulfur metabolism, in the liver. *Proc. West. Pharmacol. Soc.* 38, 37–40.
- (20) Yan, C. C., and Huxtable, R. J. (1996) Effects of monocrotaline, a pyrrolizidine alkaloid, on glutathione metabolism in the rat. *Biochem. Pharmacol.* 51, 375–379.
- (21) Cheng, W., Oike, M., Hirakawa, M., Ohnaka, K., Koyama, T., and Ito, Y. (2005) Excess l-arginine restores endothelium-dependent relaxation impaired by monocrotaline pyrrole. *Toxicol. Appl. Pharmacol.* 207, 187–194.
- (22) Copple, B. L., Roth, R. A., and Ganey, P. E. (2006) Anticoagulation and inhibition of nitric oxide synthase influence hepatic hypoxia after monocrotaline exposure. *Toxicology* 225, 128–137.
- (23) Conotte, R., and Colet, J. M. (2014) A metabonomic evaluation of the monocrotaline-induced sinusoidal obstruction syndrome (SOS) in rats. *Toxicol. Appl. Pharmacol.* 276, 147–156.
- (24) Xiong, A., Yang, F., Fang, L., Yang, L., He, Y., Wan, Y. Y., Xu, Y., Qi, M., Wang, X., Yu, K., Tsim, K. W., and Wang, Z. (2014) Metabolomic and genomic evidence for compromised bile acid homeostasis by senecionine, a hepatotoxic pyrrolizidine alkaloid. *Chem. Res. Toxicol.* 27, 775–786.
- (25) Suganya, N., Bhakkiyalakshmi, E., Subin, T. S., Krishnamurthi, K., Devi, S. S., Lau, K., Sekar, T. V., Paulmurugan, R., and Ramkumar, K. M. (2014) Proteomic identification of pterostilbene-mediated anticancer activities in HepG2 cells. *Chem. Res. Toxicol.* 27, 1243–1252.
- (26) Fountoulakis, M., Berndt, P., Boelsterli, U. A., Crameri, F., Winter, M., Albertini, S., and Suter, L. (2000) Two-dimensional database of mouse liver proteins: changes in hepatic protein levels following treatment with acetaminophen or its nontoxic regiosomer 3-acetamidophenol. *Electrophoresis* 21, 2148–2161.
- (27) Fountoulakis, M., and Suter, L. (2002) Proteomic analysis of the rat liver. *J. Chromatogr. B: Anal. Technol. Biomed. Life Sci.* 782, 197–218.
- (28) Stamper, B. D., Mohar, I., Kavanagh, T. J., and Nelson, S. D. (2011) Proteomic analysis of acetaminophen-induced changes in mitochondrial protein expression using spectral counting. *Chem. Res. Toxicol.* 24, 549–558.
- (29) Wang, Z. Y., Kang, H., Ji, L. L., Yang, Y. Q., Liu, T. Y., Cao, Z. W., Morahan, G., and Wang, Z. T. (2012) Proteomic characterization of the possible molecular targets of pyrrolizidine alkaloid isoline-induced hepatotoxicity. *Environ. Toxicol. Pharmacol.* 34, 608–617.
- (30) Stegelmeier, B. L., Edgar, J. A., Colegate, S. M., Gardner, D. R., Schoch, T. K., Coulombe, R. A., and Molyneux, R. J. (1999) Pyrrolizidine alkaloid plants, metabolism and toxicity. *J. Nat. Toxins* 8, 95–116.
- (31) de Jonge, M. E., Huitema, A. D., Beijnen, J. H., and Rodenhuis, S. (2006) High exposures to bioactivated cyclophosphamide are related to the occurrence of veno-occlusive disease of the liver following high-dose chemotherapy. *Br. J. Cancer* 94, 1226–1230.
- (32) Poreddy, V., and DeLeve, L. D. (2002) Hepatic circulatory diseases associated with chronic myeloid disorders. *Clin. Liver. Dis.* 6, 909–931.
- (33) DeLeve, L. D. (2001) Hepatic venoocclusive disease: a major complication of hematopoietic stem cell transplantation in cancer patients. *Tumori* 87, S27–29.
- (34) Sigma Diagnostic (1985) Transaminase (ALT/GPT) and (AST/GOT) Procedure No. 505.
- (35) Eisen, M. B., Spellman, P. T., Brown, P. O., and Botstein, D. (1998) Cluster analysis and display of genome-wide expression patterns. *Proc. Natl. Acad. Sci. U. S. A.* 95, 14863–14868.
- (36) Zhang, Z. X., Lu, C., Liu, X. R., Su, J., Dai, W. X., Yan, S. K., Lu, A. P., and Zhang, W. D. (2014) Global and Targeted Metabolomics Reveal That Bupleurotoxin, a Toxic Type of Polyacetylene, Induces Cerebral Lesion by Inhibiting GABA Receptor in Mice. *J. Proteome. Res.* 13, 925–933.
- (37) Sapeika, N., and Parker, R. G. (1953) Effect of senecio alkaloid pterophine on the structure and the ascorbic acid of the rat liver. *S. Afr. J. Med. Sci.* 18, 1–4.
- (38) White, I. N., Mattocks, A. R., and Butler, W. H. (1973) The conversion of the pyrrolizidine alkaloid retrorsine to pyrrolic derivatives in vivo and in vitro and its acute toxicity to various animal species. *Chem.-Biol. Interact.* 6, 207–218.
- (39) van der Watt, J. J., Purchase, I. F., and Tustin, R. C. (1972) The chronic toxicity of retrorsine, a pyrrolizidine alkaloid, in vervet monkeys. *J. Pathol.* 107, 279–287.
- (40) Wang, C. C., Xia, Q., Li, M., Wang, S., Zhao, Y., Tolleson, W. H., Yin, J. J., and Fu, P. P. (2014) Metabolic Activation of Pyrrolizidine Alkaloids Leading to Phototoxicity and Photogenotoxicity in Human HaCaT Keratinocytes. *J. Environ. Sci. Heal. C* 32, 362–384.
- (41) Afzelius, B. A., and Schoental, R. (1967) The ultrastructure of the enlarged hepatocytes induced in rats with a single oral dose of retrorsine, a pyrrolizidine (Senecio) alkaloid. *J. Ultrastruct. Res.* 20, 328–345.
- (42) Mingatto, F. E., Maioli, M. A., Bracht, A., and Ishii-Iwamoto, E. L. (2008) Effects of monocrotaline on energy metabolism in the rat liver. *Toxicol. Lett.* 182, 115–120.
- (43) Cao, W., Cao, J., Huang, J., Yao, J., Yan, G., Xu, H., and Yang, P. (2013) Discovery and confirmation of O-GlcNAcylated proteins in rat liver mitochondria by combination of mass spectrometry and immunological methods. *PLoS One* 8, e76399.
- (44) Martinez, A. I., Perez-Arellano, I., Pekkala, S., Barcelona, B., and Cervera, J. (2010) Genetic, structural and biochemical basis of carbamoyl phosphate synthetase 1 deficiency. *Mol. Genet. Metab.* 101, 311–323.
- (45) Xu, C. F., Zhang, X. Q., Yu, C. H., Lu, G. H., Chen, S. H., Xu, L. M., Ding, W., Shi, Q. J., and Li, Y. M. (2009) Proteomic analysis of hepatic ischemia/reperfusion injury and ischemic preconditioning in mice revealed the protective role of ATP5 beta. *Proteomics* 9, 409–419.
- (46) Kallianpur, A. R., Hall, L. D., Yadav, M., Byrne, D. W., Speroff, T., Dittus, R. S., Haines, J. L., Christman, B. W., and Summar, M. L. (2005) The hemochromatosis C282Y allele: a risk factor for hepatic veno-occlusive disease after hematopoietic stem cell transplantation. *Bone Marrow Transplant.* 35, 1155–1164.
- (47) Pekkala, S., Martinez, A. I., Barcelona, B., Yefimenko, I., Finckh, U., Rubio, V., and Cervera, J. (2010) Understanding carbamoyl-phosphate synthetase I (CPS1) deficiency by using expression studies and structure-based analysis. *Hum. Mutat.* 31, 801–808.
- (48) DeLeve, L. D. (2013) Liver sinusoidal endothelial cells and liver regeneration. *J. Clin. Invest.* 123, 1861–1866.

- (49) Pearson, D. L., Dawling, S., Walsh, W. F., Haines, J. L., Christman, B. W., Bazyk, A., Scott, N., and Summar, M. L. (2001) Neonatal pulmonary hypertension–urea-cycle intermediates, nitric oxide production, and carbamoyl-phosphate synthetase function. *N. Engl. J. Med.* 344, 1832–1838.
- (50) Pieczenik, S. R., and Neustadt, J. (2007) Mitochondrial dysfunction and molecular pathways of disease. *Exp. Mol. Pathol.* 83, 84–92.
- (51) Butow, R. A. (2002) Cellular responses to mitochondrial dysfunction: it's not always downhill. *Cell Death Differ.* 9, 1043–1045.
- (52) Maioli, M. A., Alves, L. C., Perandin, D., Garcia, A. F., Pereira, F. T., and Mingatto, F. E. (2011) Cytotoxicity of monocrotaline in isolated rat hepatocytes: effects of dithiothreitol and fructose. *Toxicol.* 57, 1057–1064.
- (53) Mingatto, F. E., Dorta, D. J., dos Santos, A. B., Carvalho, I., da Silva, C. H., da Silva, V. B., Uyemura, S. A., dos Santos, A. C., and Curti, C. (2007) Dehydromonocrotaline inhibits mitochondrial complex I. A potential mechanism accounting for hepatotoxicity of monocrotaline. *Toxicol.* 50, 724–730.
- (54) Zhang, X. Q., Xu, C. F., Yu, C. H., Lu, G. H., Chen, S. H., Xu, L. M., Ding, W., Shi, Q. J., and Li, Y. M. (2008) Proteomic analysis of hepatic ischemia/reperfusion injury and ischemic preconditioning in mice revealed the protective role of Atp5b. *Gastroenterology* 134, A805–A805.
- (55) Arakaki, N., Nagao, T., Niki, R., Toyofuku, A., Kuramoto, Y., Emoto, Y., and Higuti, T. (2004) Possible role of cell surface H+-ATP synthase in the extracellular ATP synthesis and proliferation of human umbilical vein endothelial cells. *Faseb. J.* 18, C105–C105.
- (56) Arakaki, N., Nagao, T., Niki, R., Toyofuku, A., Tanaka, H., Kuramoto, Y., Emoto, Y., Shibata, H., Magota, K., and Higuti, T. (2003) Possible role of cell surface H+-ATP synthase in the extracellular ATP synthesis and proliferation of human umbilical vein endothelial cells. *Mol. Cancer. Res.* 1, 931–939.
- (57) Moser, T. L., Stack, M. S., Asplin, I., Enghild, J. J., Hojrup, P., Everitt, L., Hubchak, S., Schnaper, H. W., and Pizzo, S. V. (1999) Angiostatin binds ATP synthase on the surface of human endothelial cells. *Proc. Natl. Acad. Sci. U. S. A.* 96, 2811–2816.
- (58) Titz, B., Elamin, A., Martin, F., Schneider, T., Dijon, S., Ivanov, N. V., Hoeng, J., and Peitsch, M. C. (2014) Proteomics for systems toxicology. *Comput. Struct. Biotechnol. J.* 11, 73–90.
- (59) Heijne, W. H., Kienhuis, A. S., van Ommen, B., Stierum, R. H., and Grotens, J. P. (2005) Systems toxicology: applications of toxicogenomics, transcriptomics, proteomics and metabolomics in toxicology. *Expert Rev. Proteomics* 2, 767–780.

■ NOTE ADDED AFTER ASAP PUBLICATION

This paper was published ASAP on August 17, 2015. Figures 2 and 5 have been replaced. The corrected version was reposted on August 20, 2015.